



Semnan University



Natural Convection Heat Transfer of Ag-MgO/Water Micropolar Hybrid Nanofluid Inside an F-Shaped Cavity Equipped by Hot Obstacle

Rasul Mohebbi^{*,a}, Abbas Abbaszadeh^a, Mahsa Varzandeh^a, Yuan Ma^{*,b,c}

^aSchool of Engineering, Damghan University, Damghan 3671641167, Iran

^bDepartment of Mechanical Engineering, The Hong Kong Polytechnic University, Hong Kong, China

^cShanghai Automotive Wind Tunnel Center, Tongji University, No.4800, Cao'an Road, Shanghai 201804, China

PAPER INFO

Paper history:

Received: 2020-09-03

Revised: 2021-07-03

Accepted: 2021-07-08

Keywords:

Nanofluid;
Hot obstacle;
Lattice Boltzmann Method;
Natural convection;
F-shaped cavity.

ABSTRACT

This paper presents a series of numerical simulations of nanofluid natural convection inside an F-shaped enclosure equipped by heat source. A hybrid nanofluid consisting of Ag and MgO nanoparticles and water as base fluid was used. Lattice Boltzmann method (LBM) was applied and the effects of Raleigh number ($10^3 \leq Ra \leq 10^6$), solid volume fraction of nanoparticle ($0 \leq \phi \leq 0.02$), and heat source location ($0 \leq S \leq 0.9$) on the flow field, distribution of temperature and heat transfer performance were analyzed according to streamlines, isotherms, and profiles of average Nusselt numbers. The results indicated that the average Nusselt number enhances by increasing the ϕ , although the addition of nanoparticles cannot change the flow pattern and the thermal field significantly. At low Ra, the effect of Ra on average Nu is weak. However, for high Ra, the heat transfer increases significantly by increasing the Ra. The position of heat source also affects the average Nu. The $S = 0.6$ is the best position of the hot obstacle for enhancing the heat transfer and $S = 0.9$ is the worst choice. This trend cannot be affected by Ra and ϕ .

DOI: 10.22075/JHMTR.2021.21269.1303

© 2021 Published by Semnan University Press. All rights reserved.

1. Introduction

Heat transfer of natural convection has been widely used in many engineering applications due to its easiness, low cost, small size, and dependability of heat transfer. The natural convection in cavities has attracted more and more attention in the past few decades[1,2]. From another perspective, because of the lack of energy, improving energy efficiency is most important. In the heat transfer's field, the applications of nanofluids enhance heat transfer and reduce the waste of energy[3,4]. Therefore, it is natural to think of using nanofluids to enhance the natural convection heat transfer in the enclosures. Alloui et al.[5] studied nanofluid natural convection in a rectangular enclosure. In their work, two horizontal walls were Neumann boundary conditions and two vertical walls were insulated. According to the results, the authors considered that nanofluid reduces the flow strength and the

phenomenon is more evident at lower Rayleigh number. Natural convection heat transfer of nanofluid studied by Sheikhzadeh et al.[6] in a square cavity. They found that the average Nusselt number increases by augmentation of Ra and ϕ . Besides, for the different Ra, the locations of thermal active parts for maximum average Nusselt numbers are different.

In addition to regular rectangular cavities, the nanofluids heat transfer of natural convection in irregularly shaped cavities has also been extensively studied. Sheremet et al.[7] investigated Cu/water nanofluid heat transfer in an inclined wavy cavity. In their cavity, the left bottom corner was heated and the top wavy wall was fixed at a low temperature. In addition, when the cavity inclination angle was changed, the positions of the heater and cooler were changed, which lead to the essential of fluid flow and heat transfer became different. Makulati et al.[8] investigated the Al_2O_3 /water nanofluid natural

*Corresponding Author: Rasul Mohebbi, School of Engineering, Damghan University, Damghan 3671641167, Iran.

Email: rasul_mohebbi@du.ac.ir

*Corresponding Author: Yuan Ma, Shanghai Automotive Wind Tunnel Center, Tongji University, No.4800, Cao'an Road, Shanghai 201804, China

Email: 1510812@tongji.edu.cn

Table 1. Properties of the pure fluid and the nanoparticles[28]

Property	Fluid phase (Water)	Ag	MgO
C_p (J kg ⁻¹ K ⁻¹)	4179	235	955
ρ (kg m ⁻³)	997.1	10500	3560
K (W m ⁻¹ K ⁻¹)	0.613	429	45
$\beta \times 10^5$ (K ⁻¹)	1.67	1.89	1.13
$\mu \times 10^4$ (kg m ⁻¹ s ⁻¹)	8.55		
ν (m ² s ⁻¹)	0.79		

The D₂Q₉ model was used for simulation the flow field and heat transfer. The governing equations for flow and thermal field are as follow:

$$f_i(x + e_i \Delta t, t + \Delta t) = f_i(x, t) + \frac{\Delta t}{\tau_v} [f_i^{eq}(x, t) - f_i(x, t)] + \Delta t e_i \cdot F_i \quad (7)$$

$$g_i(x + e_i \Delta t, t + \Delta t) = g_i(x, t) + \frac{\Delta t}{\tau_c} [g_i^{eq}(x, t) - g_i(x, t)] \quad (8)$$

where F is external forces and Δt denotes lattice time, g_i^{eq} and f_i^{eq} denotes the equilibrium distribution function, τ_c and τ_v indicate the temperature and flow relaxation time, respectively.

$$\tau_v = 0.5 + \nu \frac{1}{\delta t c_s^2} \quad (9)$$

$$\tau_c = 0.5 + \frac{\alpha}{c_s^2 \delta t} \quad (10)$$

where $c_s = c / \sqrt{3}$ is the speed of sound, $c=1$ and ν is kinetic viscosity. In addition, f_i^{eq}, g_i^{eq} can be found by[32]:

$$f_i^{eq} = w_i \rho [1 + \frac{e_i \cdot u}{c_s^2} + \frac{1}{2} (\frac{e_i \cdot u}{c_s^2})^2 - \frac{1}{2} \frac{u^2}{c_s^2}] \quad (11)$$

$$g_i^{eq} = w_i T [1 + \frac{c_i \cdot u}{c_s^2}] \quad (12)$$

where the ρ is the local density. The weight function w_i has the value of $w_0 = 4/9, w_{1-4} = 1/9, w_{5-8} = 1/36$ and the discrete particle velocity vectors e_i in equations (7) and (8) are defined by:

$$e_i = \begin{cases} (0,0) & (i = 0) \\ (\cos[(i-1)\pi/2], \sin[(i-1)\pi/2]) \cdot c & (i = 1, \dots, 4) \\ \sqrt{2}(\cos[(i-5)\pi/2 + \pi/4], \sin[(i-5)\pi/2 + \pi/4]) \cdot c & (i = 5, \dots, 8) \end{cases} \quad (13)$$

The force term in Eq. (7) in vertical direction (y) calculated by:

$$F_i = 3\omega_i \rho g \beta (T - T_m) \quad (14)$$

The macroscopic variables can be found by:

$$\begin{aligned} \rho &= \sum_{i=0}^8 f_i \\ \rho u &= \sum_{i=0}^8 f_i e_i \\ T &= \sum_{i=0}^8 g_i \end{aligned} \quad (15)$$

For the boundary conditions, the bounce-back scheme is used for the solid walls. In addition, the walls of obstacles and BC-DE-FG-HI walls are set to be unity ($T_h=1$) and zero ($T_c=0$), respectively. The other remaining walls (AB-AJ-JI-HG-EF-DC) imposed adiabatic.

The local Nusselt number is very important in heat transfer problems, so for the hot wall the local Nu numbers derived as:

For vertical walls:

$$Nu_n = - \left(\frac{k_{nf}}{k_f} \right) \left(\frac{\partial \theta}{\partial X} \right) \quad (16a)$$

For horizontal walls:

$$Nu_n = - \left(\frac{k_{nf}}{k_f} \right) \left(\frac{\partial \theta}{\partial Y} \right) \quad (16b)$$

where $\theta = \frac{T - T_c}{T_h - T_c}$ and the averaged Nu number

calculates by integrating the local Nu along obstacle.

3. Grid independence and code validation

For study the grid independence of homemade code by FORTRAN, three different meshes developed and the averaged Nu number calculate for $S=0$ and $\phi=0.01$ at different Ra number. The results showed in Table 2. As can be found, the grid 200×200 is appropriate for the study. The accuracy of the present numerical model checked by study of Matori et. al and a very good adoption found between the results, see Figure 2.

4. Results and discussion

Natural convection of Ag-MgO/water hybrid nanofluid inside an F-shaped cavity with a hot obstacle is studied using LBM. The effects of nanoparticle volume fraction ($0 \leq \phi \leq 0.02$), Rayleigh number ($10^3 \leq Ra \leq 10^6$) and obstacle position ($0 \leq S \leq 0.9$) on the flow pattern, temperature distribution and heat transfer performance are investigated. The results are displayed by the contour maps of streamlines and isotherms and profiles of average Nusselt number.

Figure 3 shows the effects of ϕ and Ra on the streamlines inside the cavity for $S = 0$. It is found that the fluid around the hot source is heated and moves upward. As a result, a clockwise vortex is established inside the cavity. At $Ra = 10^3$, the vortex is relatively small and locates on the bottom side of the enclosure. The fluid on the upper side of the enclosure is almost static and no obvious streamlines of the fluid can be found because at low Ra, the buoyancy force is relatively small, leading to the weak intensity of natural convection. As for $Ra = 10^6$, the vortex inside the enclosure becomes larger in size and occupies more space. Actually, the main heat transfer mechanism at low Ra is conduction heat transfer. However, at higher Ra, the natural convection caused by buoyancy force is enhanced. Thus, the occupied area by vortex becomes larger. Convection heat transfer becomes the prominent heat transfer mechanism. Besides, two secondary vortices are established inside the large vortex.

There is an interesting point that even though at the high Rayleigh number ($Ra = 10^6$), the fluid in the two horizontal parts is also almost static. This is decided by the position of heat source and thermal boundary conditions. In fact, the vertical walls (BC and FG) of two horizontal space are fixed at a low temperature, and when the heat source locates on the bottom ($S = 0$) of sidewall (AJ), vertical walls (BC and FG) and hot sources are not directly connected. Accordingly, no distinct vortex can be found inside the horizontal spaces. As for the effect of nanoparticle volume fraction on the streamlines, one can find that the flow pattern inside the enclosure does not change by increasing nanoparticle volume fraction.

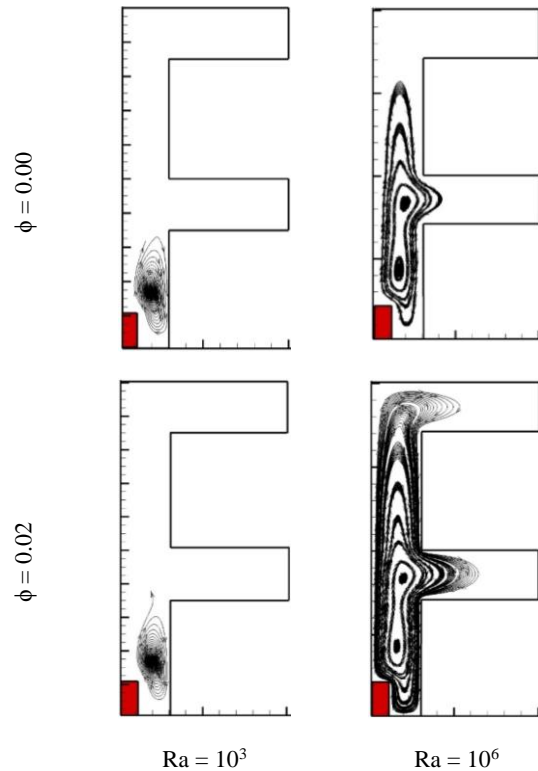


Figure 3. Effects of ϕ and Ra on the streamlines at $S=0$.

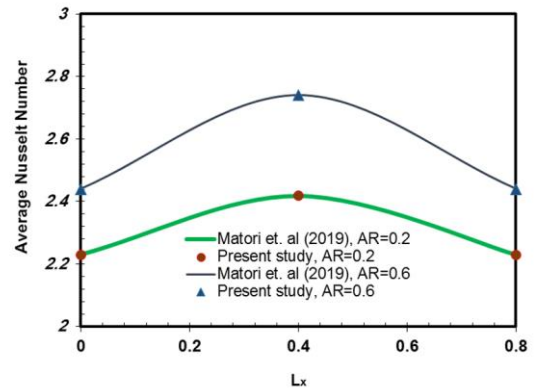


Figure 2. Comparison of average Nusselt number for the present study and Matori et. al (2019) for different aspect ratios and position at $Ra=10^6$ and $\phi=0.003$

Figure 4 displays the effects of ϕ and Ra on the temperature distribution inside the enclosure. At $Ra = 10^3$, when the primary heat transfer mechanism is conduction heat transfer, the isothermal lines can be found around the heat obstacle. They are smooth and equidistant. The fluid on the upper part of the enclosure is almost kept at $T = 0$, which is similar to streamlines. When the Rayleigh number increases to $Ra = 10^6$, the isothermal lines diffuse towards the upper part and become crooked. Besides, the fluid in the two horizontal spaces becomes warm and the fluid in the low horizontal space has a higher temperature than high horizontal space, which is due to the fact that the low horizontal space is closer to the heat source. There isnt any obviuse distinctive between the pure fluid and nanofluid.

Table 2. Effect of the mesh size on average Nusselt number, $S=0$ and $\phi=0.01$

Ra	Number of nodes	Average Nusselt number	Percentage of error
			$\frac{ Nu_{new} - Nu_{old} }{Nu_{new}} \times 100$
1000	100 × 100	1.89238	1.7217
	200 × 200	1.86035	0.0344
	300 × 300	1.85971	
1000000	100 × 100	2.41684	2.4992
	200 × 200	2.35791	0.0318
	300 × 300	2.35716	

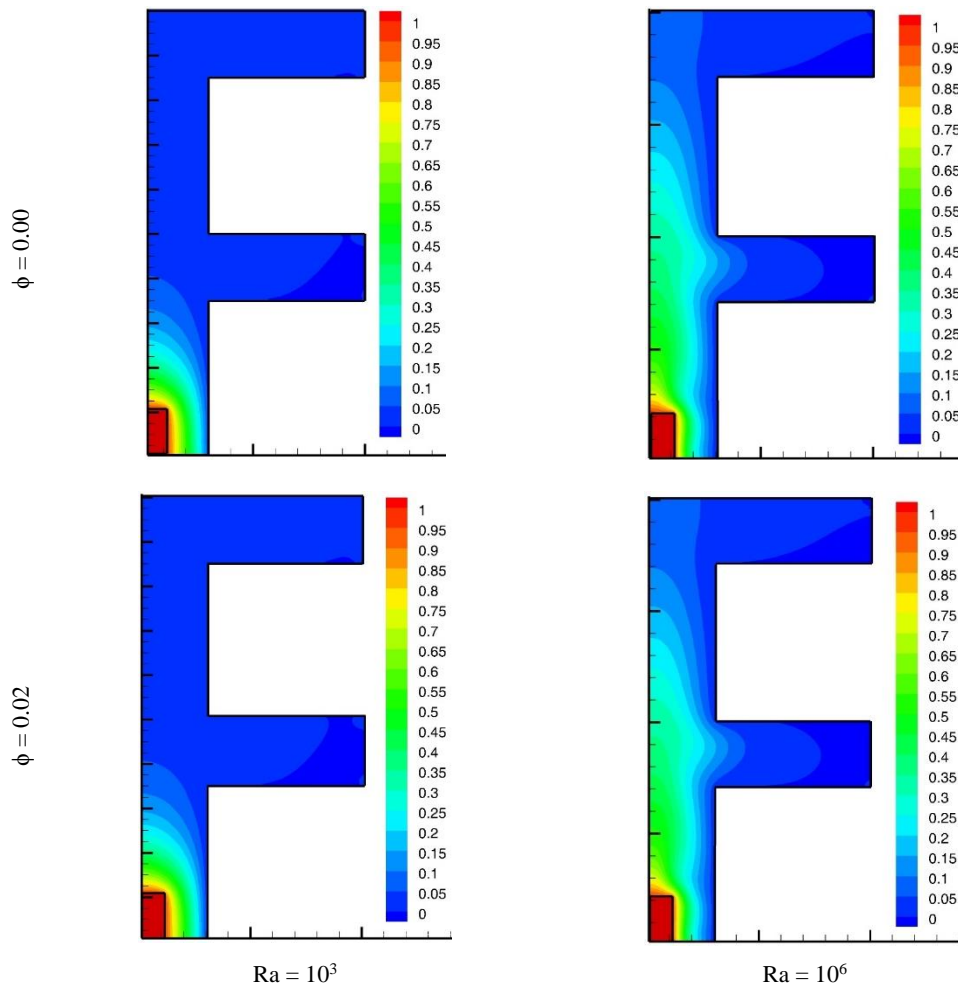


Figure 4. Effects of ϕ and Ra on the isotherms at $S=0$.

Figure 5 indicates the streamlines inside the F-shaped enclosure when the heat source moves up ($S = 0.3$) for different ϕ and Ra . In contrast to the case of $S = 0$, the flow pattern inside the enclosure changes significantly. At $Ra = 10^3$, two small vortices form adjacent to the hot obstacle. Similarly, the fluid far away from the hot obstacle is also almost static due to the conduction primary heat transfer mechanism. Compared with the flow pattern for $Ra = 10^3$ and $S = 0$, in which only one vortex can be found inside the enclosure, at $Ra = 10^3$ and $S = 0.3$, the two vortices form due to two different reasons. One can find that

when obstacle moves up, the temperature gradient between the hot obstacle and the wall DE, causes the upper vortex. The other vortex is established by the temperature difference between the hot obstacle and wall HI.

When the Ra increases to 10^6 , because of the strong natural convection, the vortex enlarges and occupies almost the whole enclosure. It should be mentioned that no secondary vortex can be found inside the large vortex and the single vortex core locates on the left top of the hot source. Because the hot obstacle is closer to the horizontal space, the fluid convection heat transfer there intensifies.

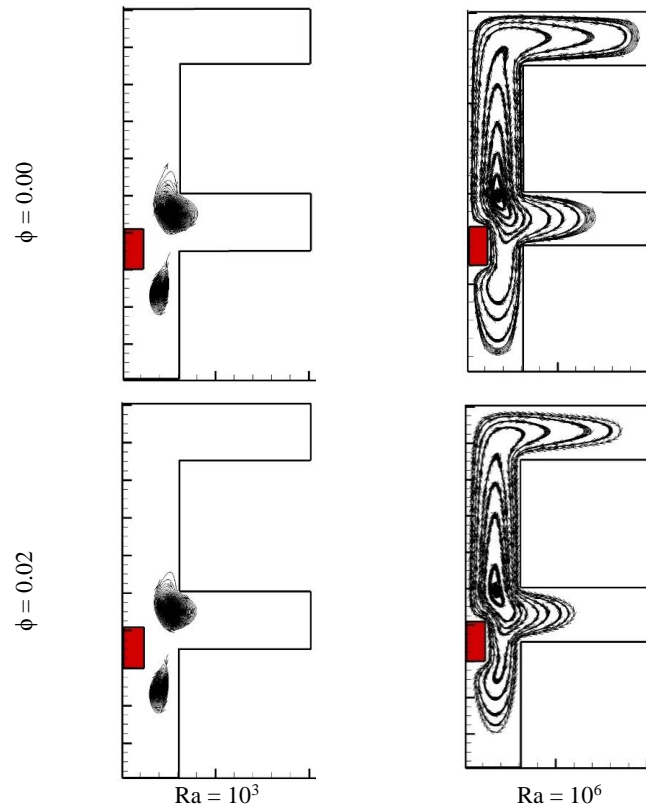


Figure 5. Effects of ϕ and Ra on the streamlines at $S=0.3$.

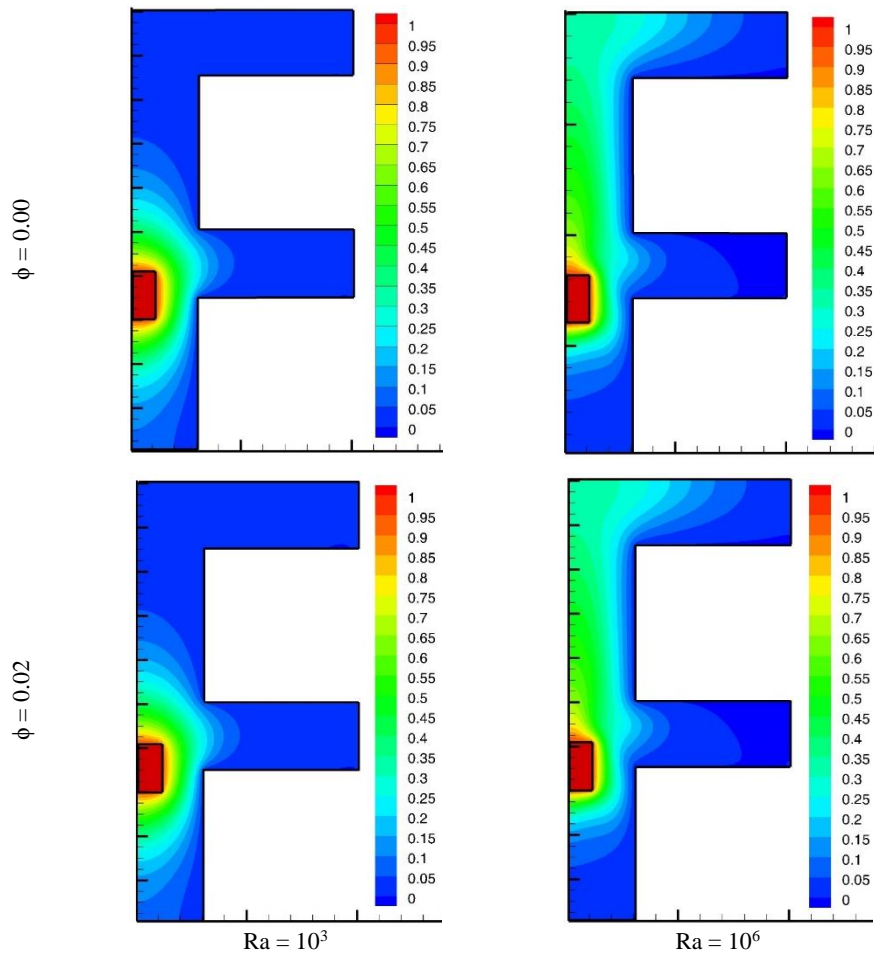


Figure 6. Effects of ϕ and Ra on the isotherms at $S=0.3$.

As for the temperature field, Figure 6 shows the isothermal lines for different ϕ and Ra at $S = 0.3$. At $Ra = 10^3$, the isothermal lines surround the hot obstacle and there is almost no difference of the isotherm gap above and below the heat source, which indicates that the temperature gradients above and below the heat source are similar. However, as Ra increasing, the convection intensity increases. It is obvious that the temperature gradient below the heat source is significantly higher than that above it. Moreover, the temperature gradient in the upper horizontal space is higher than that in the lower horizontal space. This phenomenon can be explained by the stronger vortex inside the upper horizontal space, which is shown in Figure 5.

Figure 7 presents the streamlines for different ϕ and Ra at $S = 0.6$. Due to the high value of S, the hot obstacle locates between two horizontal spaces. At $Ra = 10^3$, a vortex is established on the right of the obstacle. Due to the small gap between the heat source and wall DE, the vortex takes the shape of a dumbbell and two secondary vortices can be found inside the vortex. Moreover, due to the weak convection, the vortex is almost symmetrical. The flow pattern inside the F-shaped enclosure shows that

fluid in the lower part of the cavity cannot affect the upper fluid flow pattern. That's to say, at $Ra = 10^3$, the flow pattern in the F-shaped enclosure is similar to that inside the C-shaped enclosure. As the Rayleigh number becomes 10^6 , the flow pattern changes significantly. One large vortex forms adjacent to the hot obstacle and occupies the upper region of the cavity. No secondary can be found inside the large vortex. Besides, one small vortex can be found in the lower horizontal space. Different from the clockwise large vortex, the smaller vortex is anticlockwise. This is due to the fluid viscosity and the larger vortex drags the smaller vortex.

Figure 8 shows the effect of ϕ and Ra on the isotherms at $S=0.6$. When the Rayleigh number is 10^3 , the isothermal lines are almost symmetrical. The fluid in three regions, including two horizontal spaces and one lower region of the enclosure, are static, whose temperature is close to 0. For $Ra = 10^6$, the symmetry of isothermal lines disappear, and the isotherms below and on the right of the hot obstacle are more crowded. The temperature gradient above the obstacle is relatively small. The fluid temperature in the upper horizontal space is higher than that in the lower horizontal space.

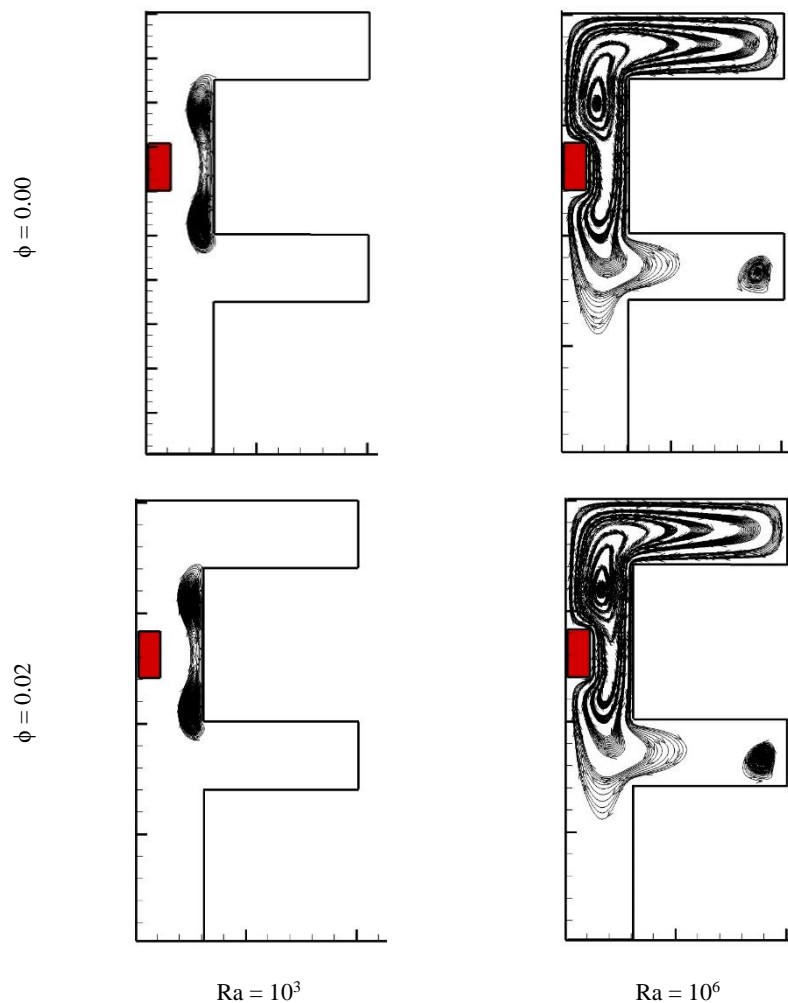


Figure 7. Effects of ϕ and Ra on the streamlines at $S=0.6$.

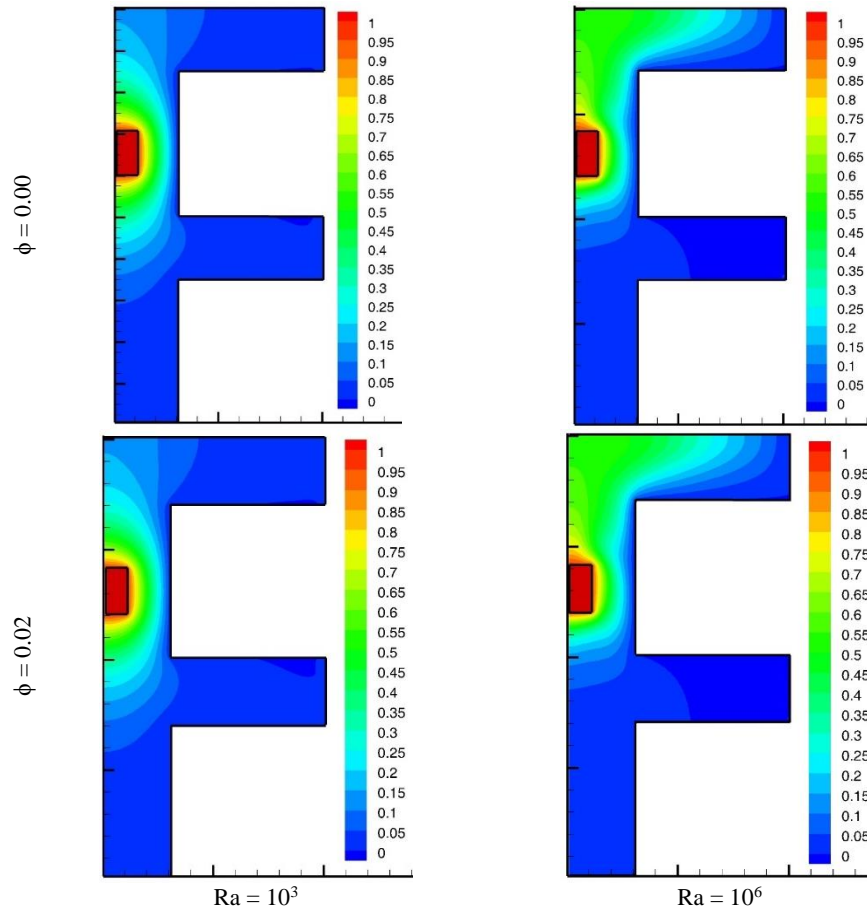


Figure 8. Effects of ϕ and Ra on the isotherms at $S=0.6$.

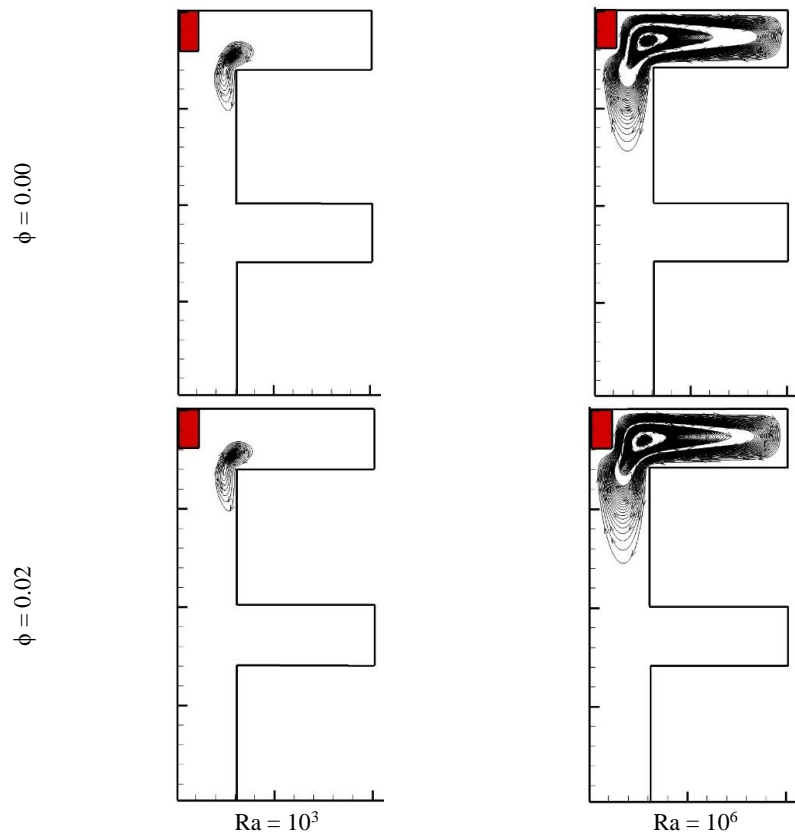


Figure 9. Effects of ϕ and Ra on the streamlines at $S=0.9$.

Figure 9 and Figure 10 show the effect of ϕ and Ra on the streamlines and isothermal lines at $S=0.9$, respectively. Due to the high location of hot obstacle ($S = 0.9$), the positions of the vortices for different Rayleigh numbers (10^3 and 10^6) are same. For $Ra = 10^6$, when the buoyancy force caused by temperature difference is large, the natural convection in other regions except the upper horizontal space is also weak. This is because, except wall BC, the other cold walls (DE, FG, and HI) locate lower than the heat source, which means the direction of the temperature gradient is same to the direction of gravity force. However, for the upper horizontal space, the obvious vortex can be found. As for the temperature distribution, one can found that the difference between isotherms for $Ra = 10^3$ and $Ra = 10^6$ at $S = 0.9$ is not as significant as those at $S = 0-0.6$. This is since the weak convection heat transfer when the hot obstacle locates on the top wall ($S = 0.9$).

Figure 11 presents the variations of average Nusselt numbers by Rayleigh number and S at different nanoparticle volume fractions. The Ra, ϕ , and S affect the average Nusselt number significantly. By increasing Ra,

the average Nu increases, but the growth trend relies on the Rayleigh number. At low Rayleigh number ($10^3 \leq Ra \leq 10^5$), the Rayleigh number influence average Nusselt number weakly. This is a consequence of the primary conduction heat transfer mechanism. When conduction is more important than convection on heat transfer, the effect of changing Ra on heat transfer by affecting convection can be neglected. However, as $Ra = 10^6$, the primary heat transfer mechanism is convection. As a result, the heat transfer increases significantly by increasing Rayleigh number. As for the nanoparticle volume fraction, one can found that the average Nusselt number increases by increasing ϕ , regardless of Ra and S.

When the position of heat source changes, the average Nusselt number changes significantly. The order of the average Nusselt number for different S is ($S = 0.6$) > ($S = 0.3$) > ($S = 0$) > ($S = 0.9$). This trend cannot be affected by Ra and ϕ . When $S = 0.6$, the heat source locates between two horizontal spaces with cold walls (BC and FG). Consequently, this arrangement is good for the heat transfer of heat source. However, at $S = 0.9$, the position of heat source is higher than the cold walls and the convection heat transfer is impeded. Therefore, its average Nusselt number is the least.

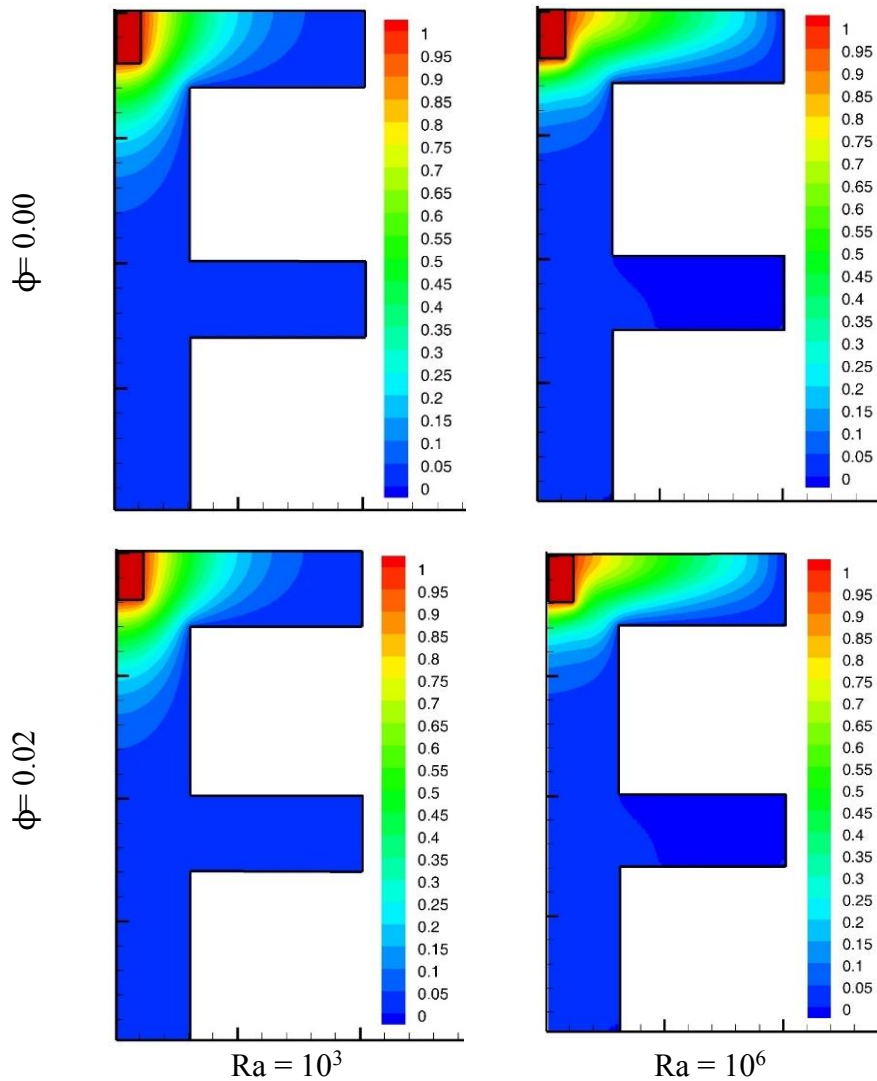


Figure 10. Effects of ϕ and Ra on the isotherms at $S=0.9$.

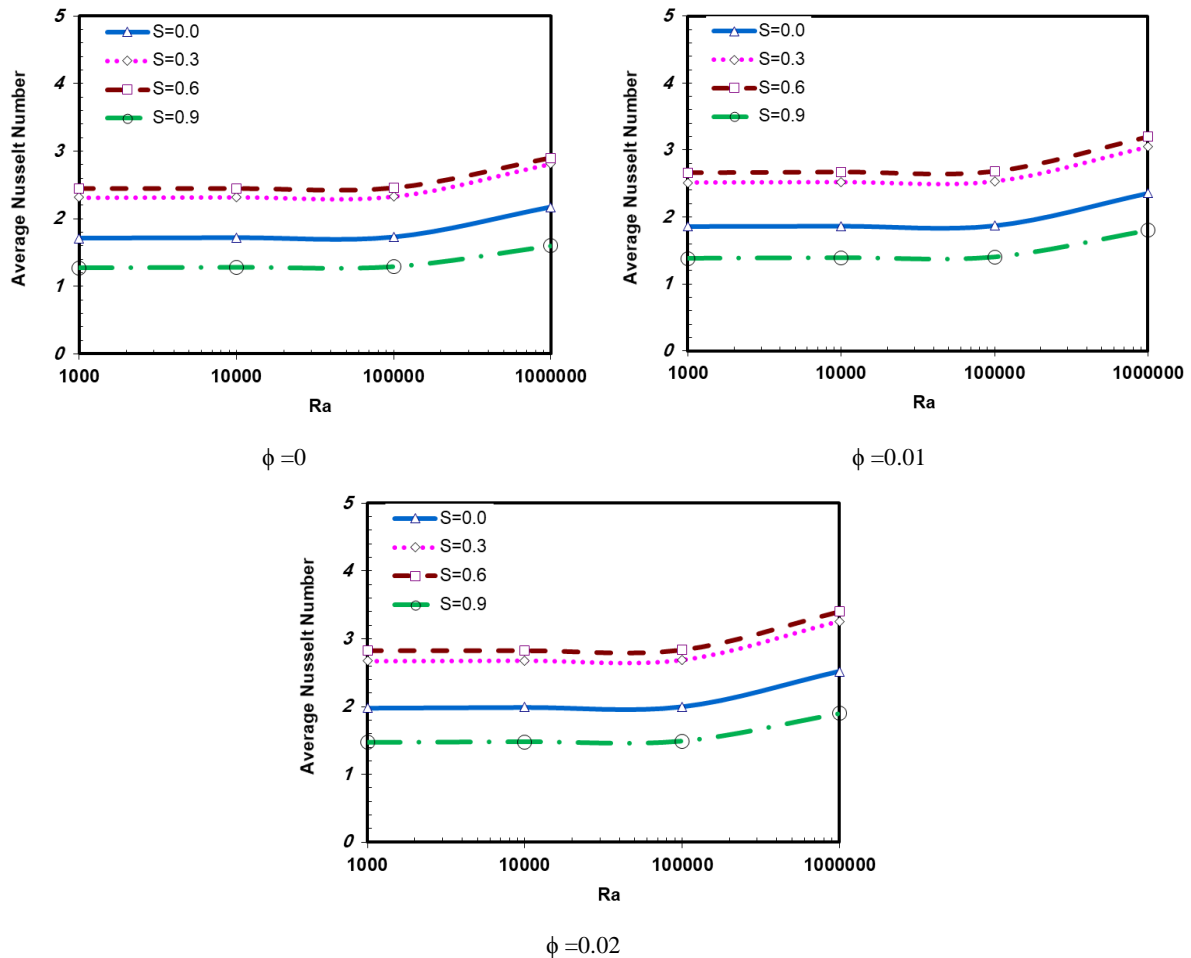


Figure 11. Effects of Ra and S on the average Nusselt number at different ϕ .

5. Conclusion

All figures and tables should be numbered with Arabic numerals and must be mentioned in the manuscript. They must be placed as close as possible to the first reference to them in the paper. In figures, number and caption should be typed below and in tables those should be typed above. Figures and tables must be aligned in the center of column and sized appropriately as width as one column. Although, large figures and tables that takes up more than 1 column width should be placed at the top or bottom of a page.

In the present research, the Ag-MgO/water hybrid nanofluid natural convection inside an F-shaped enclosure with a heat source was simulated by the LBM. The effects of Ra, ϕ and heat source location on the flow pattern, temperature distribution and heat transfer performance were investigated. To demonstrate the flow field and heat transfer characteristics, the streamlines, isotherms and profiles of average Nusselt numbers were introduced. The results showed that:

1. The average Nu increases by increasing ϕ and the addition of nanoparticles into the base fluid cannot change the flow pattern and the thermal field significantly.
2. The heat transfer performance can be enhanced when increasing Ra by intensifying the convection heat

transfer. At low Ra ($10^3 \leq Ra \leq 10^5$), the effect of Rayleigh number on average Nu is weak. However, as $Ra = 10^6$, the heat transfer increases significantly by increasing Ra.

3. The position of heat source affects the average Nusselt number significantly. $S = 0.6$ is the best position of the hot obstacle for heat transfer and $S = 0.9$ is the worst choice. This trend cannot be affected by Ra and ϕ .

Conflict of Interest Statement

There is no conflict of interest.

Nomenclature

a, b	length and height of obstacle, respectively
AR	the obstacle aspect ratio
c	lattice speed
cp	specific heat capacity at constant pressure, (J/kg K)
cs	speed of sound, (m/s)
ei	streaming speed for particle
f	density distribution function

f_{eq}	equilibrium density distribution function
g	energy distribution function
H, W	Height and length of cavity, respectively
I	Exergy destruction rate [KJ/Kg]
g_{eq}	equilibrium energy distribution function
k	thermal conductivity, (W/mK)
Nu	Nusselt number
Pr	Prandtl number
S	position of hot obstacle
T	fluid temperature, K
t	Time, s
u	velocity vector, (m/s)
x	Cartesian coordinates, m
Greek symbols	
ω_i	weight function in direction i
ϕ	solid volume fraction of nanoparticles
τ_c	relaxation time for heat transfer
α	thermal diffusivity, (m ² /s)
ρ	density, (kg /m ³)
τ_v	relaxation time for flow
μ	dynamic viscosity, (kg/ms)
Subscripts	
f	fluid
H	Hot
i	move direction of single-particle

References

- [1] Rahimi A, Saeed AD, Kasaeipoor A, Malekshah EH. A comprehensive review on natural convection flow and heat transfer. *International Journal of Numerical Methods for Heat & Fluid Flow*. 2019 Mar 4.
- [2] Amber I, O'Donovan TS. Natural convection induced by the absorption of solar radiation: A review. *Renewable and Sustainable Energy Reviews*. 2018 Feb 1;82:3526-45.
- [3] Ganvir RB, Walke PV, Kriplani VM. Heat transfer characteristics in nanofluid—a review. *Renewable and Sustainable Energy Reviews*. 2017 Aug 1;75:451-60.
- [4] Liang G, Mudawar I. Review of single-phase and two-phase nanofluid heat transfer in macro-channels and micro-channels. *International Journal of Heat and Mass Transfer*. 2019 Jun 1;136:324-54.
- [5] Alloui Z, Vasseur P, Reggio M. Natural convection of nanofluids in a shallow cavity heated from below. *International journal of Thermal sciences*. 2011 Mar 1;50(3):385-93.
- [6] Sheikhzadeh GA, Arefmanesh A, Kheirkhah MH, Abdollahi R. Natural convection of Cu-water nanofluid in a cavity with partially active side walls. *European Journal of Mechanics-B/Fluids*. 2011 Mar 1;30(2):166-76.
- [7] Sheremet MA, Oztop HF, Pop I. MHD natural convection in an inclined wavy cavity with corner heater filled with a nanofluid. *Journal of Magnetism and Magnetic Materials*. 2016 Oct 15;416:37-47.
- [8] Makulati N, Kasaeipoor A, Rashidi MM. Numerical study of natural convection of a water-alumina nanofluid in inclined C-shaped enclosures under the effect of magnetic field. *Advanced Powder Technology*. 2016 Mar 1;27(2):661-72.
- [9] Almeshaal MA, Kalidasan K, Askari F, Velkennedy R, Alsagri AS, Kolsi L. Three-dimensional analysis on natural convection inside a T-shaped cavity with water-based CNT-aluminum oxide hybrid nanofluid. *Journal of Thermal Analysis and Calorimetry*. 2020 Feb;139(3):2089-98.
- [10] Kalidasan K, Velkennedy R, Kanna PR. Laminar natural convection of Copper-Titania/Water hybrid nanofluid in an open ended C-shaped enclosure with an isothermal block. *Journal of Molecular Liquids*. 2017 Nov 1;246:251-8.
- [11] Izadi M, Mohebbi R, Karimi D, Sheremet MA. Numerical simulation of natural convection heat transfer inside a \perp shaped cavity filled by a MWCNT-Fe₃O₄/water hybrid nanofluids using LBM. *Chemical Engineering and Processing-Process Intensification*. 2018 Mar 1;125:56-66.
- [12] Hatami M, Safari H. Effect of inside heated cylinder on the natural convection heat transfer of nanofluids in a wavy-wall enclosure. *International Journal of Heat and Mass Transfer*. 2016 Dec 1;103:1053-7.
- [13] Ahmed SE, Mansour MA, Rashad AM, Salah T. MHD natural convection from two heating modes in fined triangular enclosures filled with porous media using nanofluids. *Journal of Thermal Analysis and Calorimetry*. 2020 Mar;139(5):3133-49.
- [14] Esfe MH, Saedodin S, Mahmoodi M. Experimental studies on the convective heat transfer performance and thermophysical properties of MgO-water nanofluid under turbulent flow. *Experimental thermal and fluid science*. 2014 Jan 1;52:68-78.
- [15] Ali HM, Ali H, Liaquat H, Maqsood HT, Nadir MA. Experimental investigation of convective heat transfer augmentation for car radiator using ZnO-water nanofluids. *Energy*. 2015 May 1;84:317-24.
- [16] Parvar M, Saedodin S, Rostamian SH. Experimental study on the thermal conductivity and viscosity of transformer oil-based nanofluid containing ZnO

- nanoparticles. *Journal of Heat and Mass Transfer Research*. 2020 May 1;7(1):77-84.
- [17] Kefayati GR, Hosseinizadeh SF, Gorji M, Sajjadi H. Lattice Boltzmann simulation of natural convection in tall enclosures using water/SiO₂ nanofluid. *International Communications in Heat and Mass Transfer*. 2011 Jul 1;38(6):798-805.
- [18] Ghasemi B, Aminossadati SM. Natural convection heat transfer in an inclined enclosure filled with a water-CuO nanofluid. *Numerical Heat Transfer, Part A: Applications*. 2009 Apr 16;55(8):807-23.
- [19] Bayareh M, Afshar N. Forced convective heat transfer of non-Newtonian CMC-based CuO nanofluid in a tube. *Journal of Heat and Mass Transfer Research*. 2020 Oct 1;7(2):155-63.
- [20] Dibaei M, Kargarsharifabad H. New achievements in Fe₃O₄ nanofluid fully developed forced convection heat transfer under the effect of a magnetic field: An experimental study. *Journal of Heat and Mass Transfer Research*. 2017 Apr 1;4(1):1-1.
- [21] Kumar MS, Vasu V, Gopal AV. Thermal conductivity and rheological studies for Cu-Zn hybrid nanofluids with various basefluids. *Journal of the Taiwan Institute of Chemical Engineers*. 2016 Sep 1;66:321-7.
- [22] Toghraie D, Chaharsoghi VA, Afrand M. Measurement of thermal conductivity of ZnO-TiO₂/EG hybrid nanofluid. *Journal of Thermal Analysis and Calorimetry*. 2016 Jul 1;125(1):527-35.
- [23] Hassan M, Marin M, Ellahi R, Alamri SZ. Exploration of convective heat transfer and flow characteristics synthesis by Cu-Ag/water hybrid-nanofluids. *Heat Transfer Research*. 2018;49(18).
- [24] Ghalambaz M, Doostani A, Izadpanahi E, Chamkha AJ. Conjugate natural convection flow of Ag-MgO/water hybrid nanofluid in a square cavity. *Journal of Thermal Analysis and Calorimetry*. 2020 Feb 1;139(3):2321-36.
- [25] Shahsavar A, Sardari PT, Toghraie D. Free convection heat transfer and entropy generation analysis of water-Fe₃O₄/CNT hybrid nanofluid in a concentric annulus. *International Journal of Numerical Methods for Heat & Fluid Flow*. 2019 Mar 4.
- [26] Mehryan SA, Kashkooli FM, Ghalambaz M, Chamkha AJ. Free convection of hybrid Al₂O₃-Cu water nanofluid in a differentially heated porous cavity. *Advanced Powder Technology*. 2017 Sep 1;28(9):2295-305.
- [27] Mollamahdi M, Abbaszadeh M, Sheikhzadeh GA. Flow field and heat transfer in a channel with a permeable wall filled with Al₂O₃-Cu/water micropolar hybrid nanofluid, effects of chemical reaction and magnetic field. *Journal of Heat and Mass Transfer Research*. 2016 Oct 1;3(2):101-14.
- [28] SHEIKHZADEH GHANBAR ALI, Mollamahdi Mahdi, ABBASZADEH MAHMOUD. Flow field and heat transfer of Ag-MgO/water micropolar hybrid nanofluid in a permeable channel. *TRANSPORT PHENOMENA IN NANO AND MICRO SCALES*. 2018 ;6(1):13-26.
- [29] Isabery, A.I., Mohebbi, R., Chamkha, A.J. et al. Impacts of magnetic field and non-homogeneous nanofluid model on convective heat transfer and entropy generation in a cavity with heated trapezoidal body. *J Therm Anal Calorim* 138, 1371–1394 (2019).
- [30] Mohsen Izadi, Rasul Mohebbi, Hasan Sajjadi, Amin Amiri Delouei, LTNE modeling of Magneto-Ferro natural convection inside a porous enclosure exposed to nonuniform magnetic field, *Physica A: Statistical Mechanics and its Applications*, Volume 535, 2019.
- [31] Yuan Ma, Rasul Mohebbi, M.M. Rashidi, Zhigang Yang, MHD convective heat transfer of Ag-MgO/water hybrid nanofluid in a channel with active heaters and coolers, *International Journal of Heat and Mass Transfer*, Volume 137, 2019, 714-726.
- [32] Ma, Y., Mohebbi, R., Rashidi, M.M. et al. MHD forced convection of MWCNT-Fe₃O₄/water hybrid nanofluid in a partially heated τ -shaped channel using LBM. *J Therm Anal Calorim* 136, 1723–1735 (2019).
- [33] Matori, A. et al. Lattice Boltzmann study of multi-walled carbon nanotube (MWCNT)-Fe₃O₄/water hybrid nanofluids natural convection heat transfer in a Π -shaped cavity equipped by hot obstacle. *J Therm Anal Calorim* 136, 2495–2508 (2019).